

Replica Holographic Quantum Error Correction

Jeffrey Morais^{a,b}, Kristan Jensen^a

^a*Department of Physics and Astronomy, University of Victoria, Victoria, BC V8W 3P6, Canada*

^b*BTQ Technologies, 16-104 555 Burrard Street, Vancouver BC, V7X 1M8 Canada*

E-mail: jmorais@uvic.ca, kristanj@uvic.ca

ABSTRACT: We propose a novel framework that unifies holographic quantum error correction with quantum error mitigation by employing symmetrized replicas of a holographic system. The central problem we address is the emergence of approximate bulk locality in AdS/CFT—a cornerstone for understanding how local bulk physics arises from the nonlocal dynamics of the boundary CFT. This issue is of paramount importance because conventional approaches, often based on topological error correction schemes, suffer from vanishing encoding rates and limited resilience when scaled up, while existing error mitigation techniques (such as virtual cooling and virtual distillation) have demonstrated *exponential* suppression of noise in isolated quantum systems. Previous investigations have attempted to reconstruct bulk operators via AdS-Rindler methods or tensor network models, yet they have not combined the complementary strengths of error correction and mitigation. In our work, we take a different approach: by replicating the holographic state and symmetrizing the copies, we amplify the dominant (ideal) component and thereby enhance the protection of logical information against local erasures. This synthesis refines the reconstruction of bulk observables from correlated, noisy boundary data.

Contents

1	Introduction	1
2	Holographic Replica Computations	2
2.1	Partition Function Replica Moment	2
2.2	Free Energy Replica Moment	6
2.3	Two Disk Rényi Information	9
3	Replica Quantum Error Correction	12
3.1	Replica QEC Simulations	16
3.1.1	Quantum Error Mitigation	16
3.1.2	Topological Quantum Error Correction	19
3.1.3	Replica Topological Quantum Error Correction	22
3.1.4	Relative Scaling Gain	26
3.2	Holographic Replica QEC	27
A	Appendix	27
A.1	Qutrit Quantum Error Correction	27
A.2	Preliminary Frameworks	27

1 Introduction

Quantum error correction (QEC) is indispensable for realizing reliable quantum technologies, yet its conventional implementations often demand significant resource overhead. In parallel, error mitigation techniques—most notably, quantum virtual cooling—have emerged as promising approaches to extract high-fidelity observables from noisy quantum states. In quantum virtual cooling, one prepares multiple copies of a state and, by entangling and symmetrizing these copies, effectively projects onto the dominant eigenstate, thereby suppressing noise and mimicking a reduction in the effective temperature (e.g., achieving an effective temperature $T_{\text{eff}} \sim T/M$ for M copies).

In the realm of holography, particularly within the Anti-de Sitter/Conformal Field Theory (AdS/CFT) correspondence, QEC acquires a natural geometric interpretation. Here, bulk gravitational degrees of freedom are redundantly encoded in boundary states in a manner analogous to quantum error-correcting codes, with the Ryu-Takayanagi prescription and its generalizations (via cosmic brane constructions) providing geometric realizations of entanglement and redundancy. This observation motivates the exploration of combining quantum error mitigation with holographic QEC: by entangling multiple copies of a holographic boundary state ρ to form a replicated state $\hat{\rho}_M = \rho^M / \text{Tr}(\rho^M)$, one can both

enhance the fidelity of the encoded information and distribute it across several replicas, thereby increasing resilience to local erasures.

Moreover, our framework is designed to probe how these enhanced QEC properties manifest in different gravitational regimes. In particular, while error correction in thermal AdS naturally supports bulk reconstruction, the situation becomes more subtle in the presence of black hole phases—where high entropy and information scrambling challenge conventional notions of error correction. By effectively shifting the temperature through replication, our multi-copy construction not only suppresses noise but also navigates the phase structure reminiscent of the Hawking–Page transition (and, by analogy, confinement–deconfinement phenomena in large N gauge theories). In this way, our approach sheds light on the interplay between noise, entropy, and error correction in both thermal and black hole-dominated phases.

In what follows, we review the principles of quantum virtual cooling and virtual distillation before extending these ideas to holographic settings. By drawing on the replica trick and cosmic brane methods, we establish a coherent picture wherein multi-replica entanglement enhances both error mitigation and the robustness of holographic QEC. This unified framework not only bridges the gap between abstract error correction protocols and their geometric incarnations in AdS/CFT but also opens new avenues for fault-tolerant quantum simulations in complex many-body and gravitational systems.

2 Holographic Replica Computations

A central technical challenge in our framework is to relate boundary and bulk quantities when multiple copies of the noisy CFT state are entangled. In this section we develop a precise mathematical framework to calculate the effects of symmetrization and virtual cooling on holographic observables, with a focus on phase transitions and their implications for quantum error correction. Our analysis is set in the context of the AdS/CFT correspondence, where the bulk geometry responds dynamically to patterns of boundary entanglement. In particular, by studying the M th *moment* of the thermal density matrix, we reveal how the replica partition function encodes a transition between phases—analogous to the Hawking–Page (or confinement–deconfinement) transition—that in turn governs the efficacy of bulk reconstruction.

2.1 Partition Function Replica Moment

Replica techniques are frequently employed in quantum virtual error mitigation (or virtual distillation) as well as in nonperturbative studies of quantum gravity. In these approaches one prepares M identical copies of a system in a thermal state and then projects onto the symmetric subspace to extract the dominant eigenstate of the density matrix. In our setup the thermal density matrix is defined by

$$\rho(\beta) = \frac{e^{-\beta H}}{Z(\beta)}, \quad (2.1)$$

where the partition function is given by the gravitational path integral

$$Z(\beta) = \int_{\mathcal{C}} \mathcal{D}g e^{-I[g]}. \quad (2.2)$$

Here the integration is performed over the configuration space \mathcal{C} of Riemannian metrics g on a compact Euclidean manifold \mathcal{M} (subject to appropriate boundary conditions, including a periodic Euclidean time of period β). The gravitational action is taken to be

$$I[g] = -\frac{1}{16\pi G_N} \int_{\mathcal{M}} d^d x \sqrt{g} (R - 2\Lambda) - \frac{1}{8\pi G_N} \int_{\partial\mathcal{M}} d^{d-1} x \sqrt{h} K, \quad (2.3)$$

where R is the Ricci scalar on \mathcal{M} , Λ is the cosmological constant, h is the induced metric on the boundary $\partial\mathcal{M}$, K is the trace of the extrinsic curvature, and G_N is Newton's constant. In the semiclassical approximation the dominant contribution to $Z(\beta)$ is given by the saddle point:

$$Z(\beta) \approx e^{-I_{\text{on-shell}}(\beta)}. \quad (2.4)$$

When M replicas are prepared, the effective state obtained by symmetrizing the M copies is proportional to $\rho(\beta)^M$, and its normalization is given by the M th *moment*,

$$\text{Tr}[\rho(\beta)^M] = \frac{Z(M\beta)}{[Z(\beta)]^M}. \quad (2.5)$$

This equality follows from the cyclicity of the trace and the definition of the partition function at inverse temperature $M\beta$.

In many gravitational theories the partition function receives contributions from distinct saddle points. In our case the dominant contributions arise from two geometries: the Euclidean black hole and thermal Anti-de Sitter (AdS) space. Thus, we write

$$Z(\beta) = Z_{\text{BH}}(\beta) + Z_{\text{AdS}}(\beta), \quad (2.6)$$

with

$$Z_{\text{BH}}(\beta) = e^{-I_{\text{BH}}(\beta)} \quad \text{and} \quad Z_{\text{AdS}}(\beta) = e^{-I_{\text{AdS}}(\beta)}. \quad (2.7)$$

For convenience we normalize by setting

$$I_{\text{AdS}}(\beta) = 0 \implies Z_{\text{AdS}}(\beta) = 1, \quad (2.8)$$

so that

$$Z(\beta) = e^{-I_{\text{BH}}(\beta)} + 1. \quad (2.9)$$

A similar relation holds at inverse temperature $M\beta$:

$$Z(M\beta) = e^{-I_{\text{BH}}(M\beta)} + 1. \quad (2.10)$$

Thus, the replica moment is explicitly given by

$$\mathcal{R}_M \equiv \frac{Z(M\beta)}{[Z(\beta)]^M} = \frac{e^{-I_{\text{BH}}(M\beta)} + 1}{(e^{-I_{\text{BH}}(\beta)} + 1)^M}. \quad (2.11)$$

We now evaluate the on-shell action $I_{\text{BH}}(\beta)$. The Euclidean black hole metric is

$$ds^2 = f(r) d\tau^2 + \frac{dr^2}{f(r)} + r^2 d\Omega_{d-1}^2, \quad (2.12)$$

with the lapse function

$$f(r) = 1 + \frac{r^2}{L^2} - \frac{\mu}{r^{d-2}}, \quad (2.13)$$

where L is the AdS curvature radius and μ is related to the black hole mass. The horizon $r = r_+$ is defined by $f(r_+) = 0$, which implies

$$\mu = r_+^{d-2} \left(1 + \frac{r_+^2}{L^2} \right). \quad (2.14)$$

Regularity of the Euclidean manifold near $r = r_+$ requires that we expand $f(r)$ as

$$f(r) \approx f'(r_+)(r - r_+). \quad (2.15)$$

Defining a new radial coordinate by

$$\rho^2 = \frac{4(r - r_+)}{f'(r_+)}, \quad (2.16)$$

the metric in the (τ, ρ) plane becomes

$$ds^2 \approx \rho^2 \left(\frac{f'(r_+)}{4} d\tau^2 \right) + d\rho^2. \quad (2.17)$$

The absence of a conical singularity at $\rho = 0$ requires that the Euclidean time τ be identified with period

$$\beta = \frac{4\pi}{f'(r_+)}. \quad (2.18)$$

The on-shell action $I_{\text{BH}}(\beta)$ is computed by evaluating the Einstein–Hilbert action together with the Gibbons–Hawking boundary term,

$$I[g] = -\frac{1}{16\pi G_N} \int_{\mathcal{M}} d^d x \sqrt{g} (R - 2\Lambda) - \frac{1}{8\pi G_N} \int_{\partial\mathcal{M}} d^{d-1} x \sqrt{h} K. \quad (2.19)$$

One performs the radial integration from $r = r_+$ to a large cutoff $r = R$ and then subtracts the corresponding thermal AdS contribution (which we have normalized to zero). After a careful evaluation—including the explicit integration of the bulk term and the boundary term—the result is

$$I_{\text{BH}}(\beta) = \frac{\Omega_{d-1} r_+^{d-1}}{4G_N} \frac{L^2 - r_+^2}{dr_+^2 + (d-2)L^2}. \quad (2.20)$$

Here, Ω_{d-1} is the volume of the unit $(d-1)$ -sphere and r_+ is determined implicitly via (2.18).

It is instructive to distinguish four regimes corresponding to the signs of $I_{\text{BH}}(\beta)$ and $I_{\text{BH}}(M\beta)$:

Case 1: If

$$\begin{aligned} I_{\text{BH}}(\beta) &> 0, \\ I_{\text{BH}}(M\beta) &> 0, \end{aligned} \quad (2.21)$$

then both $e^{-I_{\text{BH}}(\beta)}$ and $e^{-I_{\text{BH}}(M\beta)}$ are less than one. In this regime the thermal AdS saddle dominates the partition function so that

$$Z(\beta) \approx 1 \quad \text{and} \quad Z(M\beta) \approx 1, \quad (2.22)$$

implying

$$\mathcal{R}_M \approx 1. \quad (2.23)$$

Case 2: If

$$\begin{aligned} I_{\text{BH}}(\beta) &> 0, \\ I_{\text{BH}}(M\beta) &\leq 0, \end{aligned} \quad (2.24)$$

then the single-copy partition function is dominated by thermal AdS (since $e^{-I_{\text{BH}}(\beta)} < 1$) while the replicated partition function is dominated by the black hole saddle (because $e^{-I_{\text{BH}}(M\beta)} \geq 1$). In this case

$$\mathcal{R}_M \approx \frac{e^{-I_{\text{BH}}(M\beta)}}{(1 + e^{-I_{\text{BH}}(\beta)})^M}, \quad (2.25)$$

indicating nonextensive behavior due to the replica-induced phase transition.

Case 3 (Unphysical): If

$$\begin{aligned} I_{\text{BH}}(\beta) &\leq 0, \\ I_{\text{BH}}(M\beta) &> 0, \end{aligned} \quad (2.26)$$

then the single-copy partition function would be dominated by the black hole saddle while the replicated geometry is controlled by thermal AdS. However, this scenario is impossible because the required temperature limits for the Hawking–Page transition are not met.

Case 4: If

$$\begin{aligned} I_{\text{BH}}(\beta) &\leq 0, \\ I_{\text{BH}}(M\beta) &\leq 0, \end{aligned} \quad (2.27)$$

then both the single-copy and replicated partition functions are dominated by the black hole saddle, and the moment simplifies to

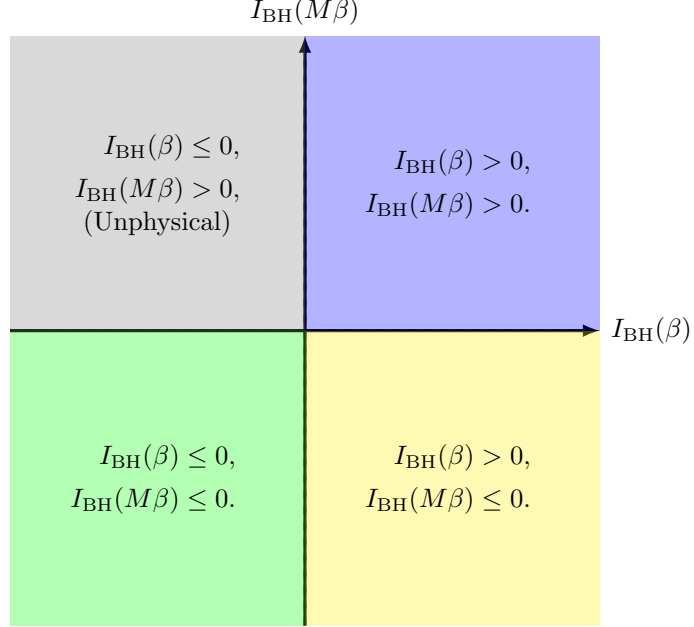
$$\mathcal{R}_M = \exp \left[-I_{\text{BH}}(M\beta) + M I_{\text{BH}}(\beta) \right]. \quad (2.28)$$

Substituting the explicit expression (2.20) into (2.11), we obtain

$$\mathcal{R}_M = \frac{\exp \left[-\frac{\Omega_{d-1} r_+^{d-1}}{4G_N} \frac{L^2 - r_+^2}{dr_+^2 + (d-2)L^2} \Big|_{M\beta} \right] + 1}{\left(\exp \left[-\frac{\Omega_{d-1} r_+^{d-1}}{4G_N} \frac{L^2 - r_+^2}{dr_+^2 + (d-2)L^2} \Big|_\beta \right] + 1 \right)^M}, \quad (2.29)$$

where in the numerator the horizon radius r_+ is determined via (2.18) with period $M\beta$ and in the denominator with β .

To visually summarize the four cases, we now present a schematic phase diagram. In the diagram the unphysical region (Case 3) is shaded in grey, while the other regions follow a scheme inspired by virid tones: yellow, green, and blue.



In the limit $M \rightarrow \infty$ the normalized replicated state

$$\hat{\rho}_M = \frac{\rho(\beta)^M}{\text{Tr}[\rho(\beta)^M]} \quad (2.30)$$

projects onto the dominant eigenstate of $\rho(\beta)$, thereby exponentially suppressing subleading contributions. This mechanism underpins the virtual distillation process central to our quantum error correction framework.

2.2 Free Energy Replica Moment

We reinterpret the thermal state in our framework as a function of the free energy:

$$\rho(\beta) := \exp\left[-\beta(H - F(\beta))\right], \quad (2.31)$$

where the free energy is defined via the partition function:

$$Z(\beta) := \text{tr}\left(e^{-\beta H}\right) \implies F(\beta) := -\frac{1}{\beta} \ln Z(\beta). \quad (2.32)$$

This definition guarantees that the shifted Hamiltonian

$$\tilde{H} := H - F(\beta) \quad (2.33)$$

satisfies the normalization condition:

$$\text{tr}\left[e^{-\beta \tilde{H}}\right] = 1. \quad (2.34)$$

In categorical language, the assignment

$$\rho : \mathbb{R}_{>0} \longrightarrow \text{End}(\mathcal{H}) \quad (2.35)$$

can be viewed as a functor from the monoidal category of positive real numbers (with multiplication) to the category **Hilb** of Hilbert spaces, while the partition function

$$Z : \beta \longmapsto \exp[-\beta F(\beta)] \quad (2.36)$$

serves as a scalar invariant encoding the thermodynamic data.

We now form M replicas by considering the tensor product:

$$\rho(\beta)^{\otimes M} \in \text{End}(\mathcal{H}^{\otimes M}). \quad (2.37)$$

Projecting onto the symmetric subobject yields the M th replica moment:

$$\mathcal{R}_M := \text{tr}[\rho(\beta)^M]. \quad (2.38)$$

Exploiting the exponential form of $\rho(\beta)$, we compute:

$$\text{tr}[\rho(\beta)^M] = \text{tr}\left[\exp\left\{-\beta M(H - F(\beta))\right\}\right] = e^{\beta M F(\beta)} Z(M\beta). \quad (2.39)$$

Noting that

$$Z(M\beta) = \exp[-M\beta F(M\beta)], \quad (2.40)$$

we arrive at the elegant expression:

$$\boxed{\mathcal{R}_M = \exp\left[-M\beta(F(M\beta) - F(\beta))\right].} \quad (2.41)$$

In the holographic context the free energy is computed from the on-shell gravitational action. In the category **Grav** of gravitational configurations, the on-shell action is given by a functor

$$I : \mathbf{Grav} \longrightarrow \mathbb{R}, \quad (2.42)$$

with the partition function expressed as:

$$Z(\beta) := e^{-I(\beta)} = e^{-I_{\text{BH}}(\beta)} + 1. \quad (2.43)$$

Thus, the free energy is explicitly:

$$F(\beta) = -\frac{1}{\beta} \ln(e^{-I_{\text{BH}}(\beta)} + 1). \quad (2.44)$$

Substituting this into the replica moment, we obtain:

$$\mathcal{R}_M = \frac{e^{-I_{\text{BH}}(M\beta)} + 1}{\left(e^{-I_{\text{BH}}(\beta)} + 1\right)^M}. \quad (2.45)$$

We now delineate the different regimes of the replica moment in terms of the free energy. For convenience, assume $\beta = 1$ so that

$$F(1) = -\ln(e^{-I_{\text{BH}}(1)} + 1). \quad (2.46)$$

Define the critical value

$$F_* := -\ln 2, \quad (2.47)$$

which corresponds to $I_{\text{BH}} = 0$. Then the regimes are defined as follows:

- **Region I:** If

$$F(1) > F_* \quad \text{and} \quad F(M) > F_*, \quad (2.48)$$

(i.e. $I_{\text{BH}}(1) > 0$ and $I_{\text{BH}}(M) > 0$), then

$$\mathcal{R}_M \approx 1. \quad (2.49)$$

- **Region II:** If

$$F(1) > F_* \quad \text{but} \quad F(M) \leq F_*, \quad (2.50)$$

(i.e. $I_{\text{BH}}(1) > 0$ and $I_{\text{BH}}(M) \leq 0$), then

$$\mathcal{R}_M \approx \frac{e^{-I_{\text{BH}}(M)}}{\left(1 + e^{-I_{\text{BH}}(1)}\right)^M}. \quad (2.51)$$

- **Region III (Unphysical):** If

$$F(1) \leq F_* \quad \text{but} \quad F(M) > F_*, \quad (2.52)$$

(i.e. $I_{\text{BH}}(1) \leq 0$ and $I_{\text{BH}}(M) > 0$), then this scenario is forbidden by the Hawking–Page transition.

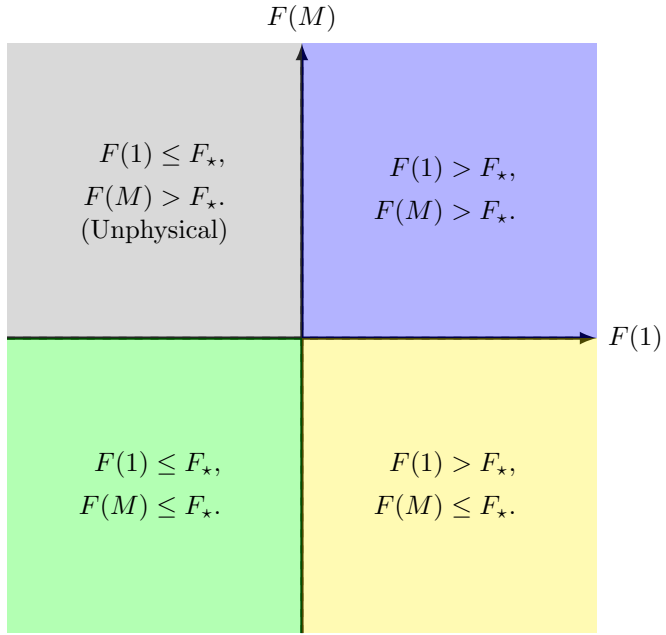
- **Region IV:** If

$$F(1) \leq F_* \quad \text{and} \quad F(M) \leq F_*, \quad (2.53)$$

(i.e. $I_{\text{BH}}(1) \leq 0$ and $I_{\text{BH}}(M) \leq 0$), then

$$\mathcal{R}_M = \exp\left[-I_{\text{BH}}(M) + M I_{\text{BH}}(1)\right]. \quad (2.54)$$

The schematic phase diagram below illustrates these regimes in the $(F(1), F(M))$ -plane. (Here we take $\beta = 1$, so that the horizontal axis is $F(1)$ and the vertical axis is $F(M)$; note that by construction $F(1)$ and $F(M)$ are negative, and the critical line is $F = -\ln 2 \approx -0.693$.)



In the limit $M \rightarrow \infty$ the normalized replicated state

$$\hat{\rho}_M := \frac{\rho(\beta)^M}{\text{tr}[\rho(\beta)^M]} \quad (2.55)$$

projects onto the dominant eigenstate of $\rho(\beta)$, thereby *purifying* the state by exponentially suppressing all subleading contributions.

This formulation—emphasizing the free energy and articulated in a categorical framework—provides an elegant, rigorous, and intuitive description of the replica moment in holographic thermal systems.

2.3 Two Disk Rényi Information

In this subsection we derive the mutual Rényi information for a configuration in which the entangling region comprises two disjoint disks on the boundary of a holographic conformal field theory. To rigorously set the stage, we interpret the boundary manifold \mathcal{M} as a smooth manifold equipped with a fibre bundle structure. In this picture, the base space corresponds to the conformal class of \mathcal{M} while the fibres represent identical copies of the local state space. The replica construction then proceeds by cyclically gluing n copies of \mathcal{M} along the entangling surface ∂A (with $A \subset \mathcal{M}$), thereby producing an n -fold branched cover $\tilde{\mathcal{M}}_n$.

For a given density matrix ρ , the Rényi entropy of order n for a region A is defined as

$$S_n(A) = \frac{1}{1-n} \ln \left(\text{Tr} (\rho_A^n) \right), \quad (2.56)$$

where ρ_A is the reduced density matrix obtained by tracing out the degrees of freedom on the complement A^c . In the holographic dual, the partition function on the branched cover,

$Z_n(A)$, is computed by evaluating the on-shell gravitational action on a bulk manifold whose asymptotic boundary is $\widetilde{\mathcal{M}}_n$. Thus, one may write

$$S_n(A) = \frac{1}{1-n} \ln \frac{Z_n(A)}{\left(Z(A)\right)^n}. \quad (2.57)$$

When the entangling region consists of two disjoint disks, labeled A_1 and A_2 , the mutual Rényi information is given by

$$I_n(A_1, A_2) = S_n(A_1) + S_n(A_2) - S_n(A_1 \cup A_2). \quad (2.58)$$

In the absence of interactions between the regions, the leading contributions cancel; however, for $n \neq 1$ the nonzero tension of the cosmic branes inserted into the bulk to implement the replica trick produces a measurable effect.

In our holographic setting, the partition function on the branched cover is obtained by introducing a cosmic brane $C^{(n)}$ whose presence modifies the bulk action. This modification obeys an area law given by

$$\tilde{S}_n \equiv n^2 \frac{\partial}{\partial n} \left(\frac{n-1}{n} S_n \right) = \frac{\text{Area}(C^{(n)})}{4G_N}, \quad (2.59)$$

where G_N is Newton's constant. The cosmic brane carries a tension

$$T_n = \frac{n-1}{4n G_N}, \quad (2.60)$$

which produces a conical deficit angle

$$\Delta\phi = 2\pi \frac{n-1}{n}. \quad (2.61)$$

For the configuration of two disks, the dominant bulk solution (when the conformally invariant cross-ratio x is below a critical value) consists of two cosmic branes, $C_1^{(n)}$ and $C_2^{(n)}$, anchored on ∂A_1 and ∂A_2 , respectively. In the absence of backreaction these surfaces do not interact and the mutual Rényi information vanishes. However, for $n \neq 1$ the nonzero tension perturbs the minimal surfaces, resulting in an area shift $\delta\mathcal{A}_i$ for each brane. To first order in $\delta n = n - 1$, the mutual Rényi information is given by

$$I_n(A_1, A_2) = -\frac{\delta\mathcal{A}_1 + \delta\mathcal{A}_2}{8G_N}. \quad (2.62)$$

To compute $\delta\mathcal{A}_1$ explicitly, we first map the region outside the first disk A_1 to the $(d-1)$ -dimensional hyperbolic space \mathbb{H}^{d-1} via a conformal transformation. This mapping is naturally formulated in terms of a fibre bundle whose base is the conformal class of the boundary metric and whose fibres are copies of \mathbb{H}^{d-1} . Let the second disk A_2 have radius R_0 ; then the cross-ratio is defined by

$$x = \frac{4R_0}{(1+R_0)^2}. \quad (2.63)$$

Under the conformal mapping, the region complementary to A_1 is equipped with the metric

$$ds^2 = d\tau^2 + d\rho^2 + \sinh^2 \rho d\Omega_{d-2}^2, \quad (2.64)$$

with the entangling surface ∂A_1 sent to $\rho \rightarrow \infty$ and A_2 mapped to the region $\rho < \rho_0$, where

$$\rho_0 = \operatorname{arctanh}\left(\frac{2R_0}{1+R_0^2}\right) = -\frac{1}{2} \ln(1-x). \quad (2.65)$$

The bulk dual of the above configuration is described by a metric of the form

$$ds_{d+1}^2 = \frac{dr^2}{f(r)} + f(r)d\tau^2 + r^2 \left(d\rho^2 + \sinh^2 \rho d\Omega_{d-2}^2 \right), \quad (2.66)$$

where r is the holographic radial coordinate and the function $f(r)$ is determined by the bulk equations of motion. In the presence of a cosmic brane with tension T_n (given by (2.60)), a conical singularity with deficit angle $\Delta\phi$ (see (2.61)) is induced in the bulk. For $n = 1$ the brane is tensionless and its location is determined by the minimal surface equation,

$$r_{n=1}(\rho) = \sqrt{\frac{1 - \tanh^2 \rho}{\tanh^2 \rho_0 - \tanh^2 \rho}}. \quad (2.67)$$

For $n \neq 1$, the nonzero tension perturbs the minimal surface, and to first order in δn the area change on the first cosmic brane is found to be

$$\delta\mathcal{A}_1 = \frac{\delta n S_{d-2} \coth \rho_0}{2(1-d)} B\left(\tanh^2 \rho_0; \frac{d+1}{2}, \frac{2-d}{2}\right), \quad (2.68)$$

where

$$S_{d-2} = \frac{2\pi^{\frac{d-1}{2}}}{\Gamma\left(\frac{d-1}{2}\right)} \quad (2.69)$$

is the volume of the unit $(d-2)$ -sphere and $B(z; a, b)$ is the incomplete beta function. By symmetry, an identical expression holds for $\delta\mathcal{A}_2$. Substituting (2.68) into (2.62) and using the holographic dictionary relation for the central charge,

$$C_T = \frac{\Gamma(d+2)}{\pi^{d/2}(d-1)\Gamma\left(\frac{d}{2}\right)} \frac{1}{8\pi G_N}, \quad (2.70)$$

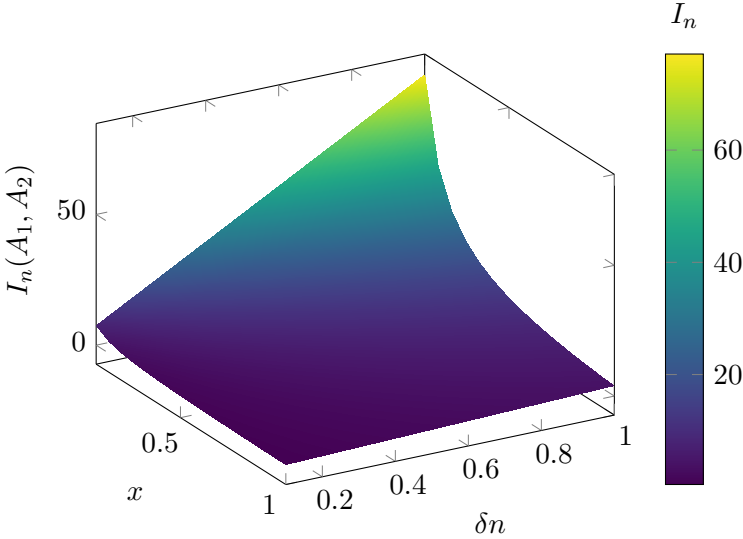
the mutual Rényi information becomes

$$I_n(A_1, A_2) = \frac{2^{3-d}\pi^{d+1}C_T \delta n}{d(d^2-1)\Gamma\left(\frac{d-1}{2}\right)^2} \frac{2-x}{x} B\left[\left(\frac{x}{2-x}\right)^2; \frac{d+1}{2}, \frac{2-d}{2}\right] + \mathcal{O}(\delta n^2). \quad (2.71)$$

To capture the intricate dependence of $I_n(A_1, A_2)$ on both the cross-ratio x and the replica deviation $\delta n = n - 1$, we now present a three-dimensional surface plot. For illustrative purposes, we set the boundary spacetime dimension to $d = 3$ and fix $C_T = 1$. In this case, equation (2.71) simplifies to

$$I_n(A_1, A_2) = \frac{\pi^4 \delta n}{24} \frac{2-x}{x}. \quad (2.72)$$

The plot below, generated using the `pgfplots` package, shows the surface $z = I_n(A_1, A_2)$ as a function of x (ranging from 0.1 to 1 to avoid the singularity at $x = 0$) and δn (ranging from 0 to 0.2).



This plot reveals the linear dependence on δn and the nonlinear dependence on the cross-ratio x , thereby illustrating the rich geometric structure that emerges from the replica construction in holographic theories.

3 Replica Quantum Error Correction

In any physical quantum system, noise and losses are unavoidable, and they lead to an inherent loss of information. When a quantum state interacts with its environment or is subjected to imperfect operations, its purity is reduced and the stored information becomes corrupted. A central goal of quantum error correction (QEC) is to prevent such information loss by encoding the desired (logical) state into a larger physical Hilbert space in which the information is spread nonlocally. In this way, even if some physical subsystems are lost or experience errors, the original logical state can still be recovered by exploiting the redundancy built into the code.

To illustrate these ideas, we consider a toy model based on a three-level quantum system (a *qutrit*). The Hilbert space for a qutrit is defined by

$$\mathcal{H} = \mathbb{C}^3 = \text{span}\{|0\rangle, |1\rangle, |2\rangle\}. \quad (3.1)$$

Here, each basis vector represents one of three distinct quantum states. We then take an arbitrary pure state in this space,

$$|\psi\rangle = \alpha|0\rangle + \beta|1\rangle + \gamma|2\rangle, \quad (3.2)$$

where the complex coefficients satisfy the normalization condition

$$|\alpha|^2 + |\beta|^2 + |\gamma|^2 = 1. \quad (3.3)$$

This state $|\psi\rangle$ is our logical state that we wish to protect against errors.

In order to repair information loss, the standard approach in QEC is to embed the logical state into a higher-dimensional space. This is achieved by an isometric map that distributes the logical information across many physical subsystems. In our model, we choose an encoding map

$$V : \mathcal{H} \rightarrow \mathcal{H}^{\otimes 3}, \quad (3.4)$$

which embeds the original qutrit into a system of three qutrits. The idea is that by “spreading” the information over three subsystems, the effect of local noise can be mitigated by recovering the original state from the remaining uncorrupted parts. For example, one may define the encoded basis states as

$$\begin{aligned} |\tilde{0}\rangle &= \frac{1}{\sqrt{3}}(|000\rangle + |111\rangle + |222\rangle), \\ |\tilde{1}\rangle &= \frac{1}{\sqrt{3}}(|012\rangle + |120\rangle + |201\rangle), \\ |\tilde{2}\rangle &= \frac{1}{\sqrt{3}}(|021\rangle + |102\rangle + |210\rangle). \end{aligned} \quad (3.5)$$

Each logical state is now encoded as an entangled state in the tensor product space $\mathcal{H}^{\otimes 3}$. The subspace

$$\mathcal{C} = \{ V|\psi\rangle : |\psi\rangle \in \mathcal{H} \} \subset \mathcal{H}^{\otimes 3} \quad (3.6)$$

serves as our code subspace. A central requirement is that this encoding satisfies the Knill–Laflamme condition. That is, for any error operator E acting on a subset of the three physical qutrits there exists a scalar $c(E)$ such that

$$\langle \tilde{i}|E^\dagger E|\tilde{j}\rangle = c(E) \delta_{ij}. \quad (3.7)$$

This relation guarantees that errors do not mix the logical basis states and hence that the logical information can be perfectly recovered provided that the error affects only a limited number of subsystems.

In a realistic scenario, however, the physical qutrits are not isolated but are instead subject to noise. To model this, suppose that each physical qutrit is independently acted upon by a depolarizing channel. This channel is defined by

$$\mathcal{E}(\rho) = (1 - p)\rho + \frac{p}{3}I_3, \quad (3.8)$$

where I_3 is the 3×3 identity and p is the probability that the state is replaced by the maximally mixed state. When this noise process acts on each of the three qutrits in the encoded state, the ideal encoded density matrix

$$\rho_{\text{ideal}} = V|\psi\rangle\langle\psi|V^\dagger \quad (3.9)$$

is transformed into a noisy state given by

$$\rho_{\text{noisy}} = (\mathcal{E} \otimes \mathcal{E} \otimes \mathcal{E})(\rho_{\text{ideal}}). \quad (3.10)$$

The performance of the code is quantified by the fidelity between the noisy state and the ideal encoded state. Using the standard definition of fidelity for a pure state and a mixed state, we have

$$F_{\text{enc}} = \langle \psi | V^\dagger \rho_{\text{noisy}} V | \psi \rangle. \quad (3.11)$$

For small values of p , one typically finds an expansion

$$F_{\text{enc}} \approx 1 - \kappa p^2, \quad (3.12)$$

where the constant $\kappa > 0$ depends on the structure of the code and the specific form of the noise. Note that even with error correction by encoding, there is a fundamental limit: if more than a certain fraction of the three physical qutrits (denoted by η_1) is lost or corrupted, the encoded logical state cannot be reliably recovered.

A further strategy to combat noise, beyond a single-copy code, is to use multiple independent copies of the encoded state and to symmetrize them. In this replica approach one prepares M copies of the noisy state, so that the overall state is

$$\rho_{\text{noisy}}^{\otimes M} = \rho_{\text{noisy}} \otimes \rho_{\text{noisy}} \otimes \cdots \otimes \rho_{\text{noisy}}, \quad (3.13)$$

where the tensor product is taken over M identical systems. One then applies a symmetrization procedure that effectively projects onto the symmetric subspace of the M copies. Mathematically, this is equivalent to forming the normalized state

$$\hat{\rho}_M = \frac{\rho_{\text{noisy}}^M}{\text{Tr}(\rho_{\text{noisy}}^M)}. \quad (3.14)$$

To explain this further, consider the spectral decomposition of the single-copy state:

$$\rho_{\text{noisy}} = \sum_{i=0}^2 \lambda_i |\phi_i\rangle\langle\phi_i|, \quad (3.15)$$

with the eigenvalues arranged in descending order so that λ_0 is associated with the ideal (error-free) component. When we take the M th power of ρ_{noisy} , we have

$$\rho_{\text{noisy}}^M = \sum_i \lambda_i^M |\phi_i\rangle\langle\phi_i|. \quad (3.16)$$

After normalization, the replicated state becomes

$$\hat{\rho}_M = \frac{\sum_i \lambda_i^M |\phi_i\rangle\langle\phi_i|}{\sum_i \lambda_i^M}. \quad (3.17)$$

The effective fidelity with respect to the ideal state is then given by

$$F_M = \langle \phi_0 | \hat{\rho}_M | \phi_0 \rangle = \frac{\lambda_0^M}{\sum_i \lambda_i^M}. \quad (3.18)$$

Assuming that the dominant eigenvalue is approximately $\lambda_0 \approx 1 - p$ and the other eigenvalues scale as $\lambda_{i \geq 1} \sim \mathcal{O}(p)$ (with $p \ll 1$), we find that the error, measured as $1 - F_M$, decays exponentially with the number of copies:

$$1 - F_M \sim \left(\frac{p}{1-p} \right)^M. \quad (3.19)$$

This result explicitly shows that by replicating the state and symmetrizing the copies the contribution from the noisy (error) components is suppressed exponentially. In other words, the effective state is purified relative to the single-copy noisy state.

Furthermore, the replication procedure enhances the robustness against physical erasures. In a single-copy code, let η_1 denote the maximum fraction of physical subsystems (here, qutrits) that can be lost while still allowing for recovery of the logical state (for the 3-qutrit code one typically requires that at most one of the three qutrits is lost). When we prepare M copies, the total number of physical subsystems is $3M$. Ideally, the redundancy from replication means that one can tolerate erasure of a fraction η_{\max} of the subsystems, where in the best case one has

$$\eta_{\max} \approx M \eta_1. \quad (3.20)$$

We then define the erasure redundancy ratio as

$$\mathcal{R}_\eta = \frac{\eta_{\max}}{\eta_1}, \quad (3.21)$$

which, in the optimal scenario, scales as $\mathcal{R}_\eta \approx M$. This metric indicates that the replicated scheme can tolerate up to M times as many erasures as a single-copy code.

An additional key ingredient in the theory of QEC is the formulation of logical operators via operator algebras. A logical operator O acting on the code subspace \mathcal{C} must have a representation that is independent of the specific physical subsystem on which it is defined. In precise terms, if X_E is any operator acting on a subset E of the physical Hilbert space, then a necessary and sufficient condition for the existence of an operator $O_{\bar{E}}$ acting solely on the complement \bar{E} (i.e. such that

$$O_{\bar{E}}|\psi\rangle = O|\psi\rangle \quad \text{for all } |\psi\rangle \in \mathcal{C} \quad (3.22)$$

is that

$$\langle \tilde{i}|[O, X_E]|\tilde{j}\rangle = 0 \quad \text{for all } i, j. \quad (3.23)$$

This operator-algebra condition ensures that the encoded (logical) information is decoupled from local disturbances. In our replicated construction the effective logical operators inherit this invariance up to corrections that vanish exponentially in M .

Thus, by first encoding a qutrit into three entangled physical qutrits using the isometric map V (which guarantees protection under the Knill–Laflamme condition) and then preparing M independent copies of the noisy encoded state followed by a symmetrization operation that produces

$$\hat{\rho}_M = \frac{\rho_{\text{noisy}}^M}{\text{Tr}(\rho_{\text{noisy}}^M)}, \quad (3.24)$$

we obtain a replicated state whose effective fidelity is

$$F_M = \frac{\lambda_0^M}{\sum_i \lambda_i^M}, \quad (3.25)$$

and which exhibits an exponential suppression of error contributions. In parallel, the tolerance to erasures is enhanced so that if a single copy tolerates the loss of a fraction η

of its subsystems, then the replicated state tolerates loss up to a fraction

$$\eta_{\max} \approx M \eta, \quad (3.26)$$

and we quantify this improvement by the erasure redundancy ratio

$$\mathcal{R}_\eta = \frac{\eta_{\max}}{\eta} \approx M. \quad (3.27)$$

This construction is rigorous and follows standard QEC theory as described in sources such as the nLab and contemporary reviews of quantum error correction. It demonstrates that by embedding logical information in a higher-dimensional space and then using multiple copies with replica symmetrization, one can both purify the effective state (enhancing fidelity) and greatly increase robustness against physical erasures, with logical operators defined via the corresponding operator algebra remaining.

3.1 Replica QEC Simulations

In this section, we provide a detailed derivation of our protocols along with their corresponding code implementations. Throughout, we use the same symbolic notation (θ , ρ_{ideal} , ρ_{noisy} , p , M , $|\psi\rangle$, etc.) and refer to the plots generated by our Python script.

3.1.1 Quantum Error Mitigation

Before describing our simulation protocol, we briefly motivate the method of virtual distillation for mitigating noise. In any realistic quantum system, unavoidable interactions with the environment degrade the state's purity and cause information loss. A common strategy to counteract this degradation is to encode the logical state into a larger Hilbert space where the information is spread nonlocally. In our approach, we not only encode the state but also prepare multiple copies, later symmetrizing them to project onto the dominant (ideal) component. This procedure—rooted in the operator-algebraic formulation of QEC—amplifies the contribution of the error-free part of the state while exponentially suppressing noisy contributions.

We begin with an ideal qubit state defined by

$$|\psi\rangle = \begin{pmatrix} \cos \theta \\ \sin \theta \end{pmatrix}, \quad (3.28)$$

and its corresponding density matrix

$$\rho_{\text{ideal}} = |\psi\rangle \langle \psi|. \quad (3.29)$$

Under a depolarizing noise channel, the state becomes mixed; we model the noisy state as

$$\rho_{\text{noisy}} = (1 - p) \rho_{\text{ideal}} + \frac{p}{2} I, \quad (3.30)$$

where I is the 2×2 identity matrix and p quantifies the probability of error. This channel captures the essence of information loss by partially replacing the pure state with maximal uncertainty.

To mitigate this loss, we employ virtual distillation by taking M copies of the noisy state and combining them via a symmetrization procedure. Mathematically, this is equivalent to forming the effective state

$$\rho_{\text{eff}} = \frac{\rho_{\text{noisy}}^M}{\text{Tr}(\rho_{\text{noisy}}^M)}. \quad (3.31)$$

Assuming that ρ_{noisy} has the spectral decomposition

$$\rho_{\text{noisy}} = \sum_i \lambda_i |\phi_i\rangle\langle\phi_i|, \quad (3.32)$$

with the eigenvalues ordered so that λ_1 is the largest (corresponding to the ideal component), raising the state to the M th power yields

$$\rho_{\text{noisy}}^M = \sum_i \lambda_i^M |\phi_i\rangle\langle\phi_i|. \quad (3.33)$$

After normalization, the effective state is

$$\rho_{\text{eff}} = \frac{\sum_i \lambda_i^M |\phi_i\rangle\langle\phi_i|}{\sum_i \lambda_i^M}. \quad (3.34)$$

We then define the fidelity between the effective state and the ideal state by

$$F = \langle\psi|\rho_{\text{eff}}|\psi\rangle = \frac{\lambda_1^M}{\lambda_1^M + \sum_{i \geq 2} \lambda_i^M}. \quad (3.35)$$

This expression demonstrates that as M increases, the contribution from the dominant eigenvalue λ_1 is exponentially amplified relative to the error components, so that F approaches unity.

In our simulations, the noise parameter p is varied and the effective fidelity F is computed for different replica counts M . The functions `createNoisyQubitDensityMatrix` and `performVirtualDistillation` are implemented to construct ρ_{noisy} as in (3.30) and to compute ρ_{eff} as in (3.31), respectively. The fidelity is then evaluated using (3.35) for each combination of p and M , confirming that the virtual distillation procedure suppresses noise exponentially and enhances the state's fidelity toward the ideal state.

Code Implementation: In our simulation, we construct the noisy qubit state using a depolarizing channel (see Equation (3.30)) and then obtain the effective state by raising this noisy state to the M th power and normalizing it as in Equation (3.31). Briefly, the simulation uses a parameter θ to define the ideal state $|\psi\rangle$, and then, for each noise level p (sampled from 0 to 1) and for each replica count M (from 1 to 10), the effective fidelity

$$F = \langle\psi|\rho_{\text{eff}}|\psi\rangle \quad (3.36)$$

is computed by iterating over the corresponding ranges. This procedure, implemented via functions that internally perform the operations described in Equations (3.30) and

(3.31), confirms that as M increases the dominant eigenvalue is amplified while the noisy contributions are suppressed.

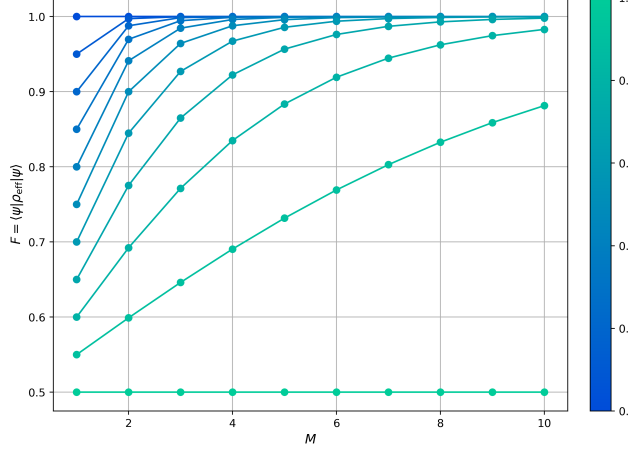


Figure 1. Fidelity Enhancement via Virtual Distillation. This plot shows the fidelity computed for noise probabilities p ranging from 0 to 1. As the replica count M increases, the effective state better approximates the ideal state because the dominant eigenvalue is exponentially amplified.

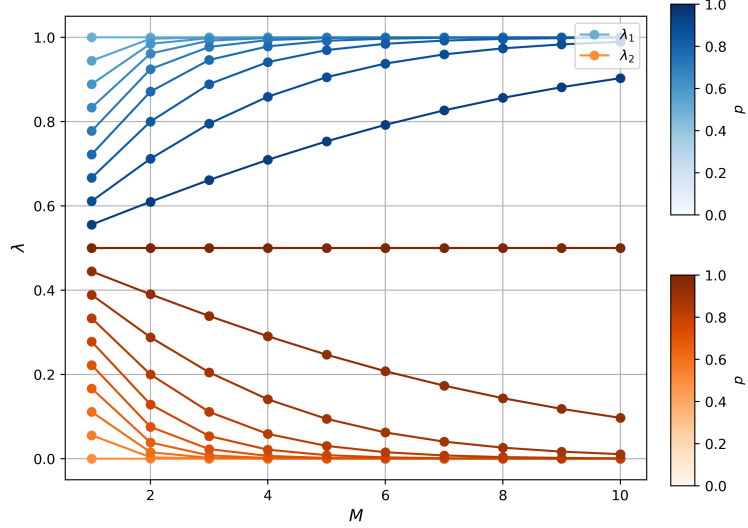


Figure 2. Eigenvalue Convergence for Multiple Noise Levels. For a representative noise probability (e.g., $p = 0.2$), the plot shows the two largest eigenvalues of the effective state ρ_{eff} as a function of M . The solid line (using a Blues gradient) represents the dominant eigenvalue λ_1 , while the dashed line (using an Oranges gradient) represents the subdominant eigenvalue λ_2 . Two gradient bars, placed to the right of the plot, indicate the mapping of noise probability p for λ_1 (ranging from 0.0 to 1.0 in the Blues palette) and for λ_2 (ranging from 0.0 to 1.0 in the Oranges palette), respectively.

3.1.2 Topological Quantum Error Correction

Kitaev's toric code is a paradigmatic example of a *stabilizer code* where logical information is encoded in global, nonlocal degrees of freedom. This nonlocal encoding protects the stored quantum information against local errors. Below we explain the fundamental principles behind the toric code and how error correction is achieved.

- **Lattice Geometry:** The toric code is defined on a two-dimensional lattice embedded on a torus. For simplicity, consider a square lattice with periodic boundary conditions. In this lattice:

- Physical qubits are placed on the *edges* of the lattice.
- Vertices (or *stars*) are labeled by v , and faces (or *plaquettes*) are labeled by p .
- For an $L \times L$ lattice, the total number of edges is $n = 2L^2$.

- **Stabilizer Operators:** Two families of commuting operators are defined on this lattice:

1. *Star (vertex) operators* A_v : For each vertex v , define

$$A_v = \prod_{e \in \partial(v)} \sigma_e^x, \quad (3.37)$$

where $\partial(v)$ denotes the set of edges incident to the vertex v , and σ_e^x is the Pauli X operator acting on the qubit on edge e .

2. *Plaquette (face) operators* B_p : For each face p , define

$$B_p = \prod_{e \in \partial(p)} \sigma_e^z, \quad (3.38)$$

where $\partial(p)$ is the set of edges surrounding the face p , and σ_e^z is the Pauli Z operator acting on edge e .

The code space is defined as the simultaneous +1 eigenstate of all the stabilizer operators:

$$\mathcal{L} = \left\{ |\Psi\rangle \in (\mathbb{C}^2)^{\otimes n} \mid A_v |\Psi\rangle = |\Psi\rangle, B_p |\Psi\rangle = |\Psi\rangle, \forall v, p \right\}. \quad (3.39)$$

This is equivalent to the ground state space of the Hamiltonian:

$$H_0 = - \sum_v A_v - \sum_p B_p. \quad (3.40)$$

Because all stabilizers commute, the code space is robust to local errors. Logical qubits are encoded in the *global* degrees of freedom of the system. In fact, on a torus (which has genus $g = 1$) the ground space is fourfold degenerate, meaning that there are two logical qubits encoded in the nonlocal properties of the state. Logical operators are nonlocal string operators that commute with all the stabilizers but act nontrivially on the code space. For example, a logical operator might consist of a product of σ^z operators along a non-contractible loop around the torus. Such an operator cannot be written as a product of the local stabilizers and therefore changes the logical state while leaving the syndrome (the measurement outcomes of the stabilizers) unchanged.

Simulation Setup In our numerical simulation, we:

1. **Initialize:** Prepare a logical qubit encoded in the toric code with $n = 2L^2$ physical qubits.
2. **Apply noise:** For each physical qubit, with probability p we apply a random X, Y , or Z (each with probability $1/3$). Equivalently, after every two-qubit gate, we place such an error on the edges that were involved, preserving the topological code structure.
3. **Syndrome extraction:** For each vertex v , compute

$$A_v(\vec{\alpha}) = \prod_{e \in \partial(v)} E(\alpha_e), \quad E(\alpha_e) = \begin{cases} +1, & \alpha_e \in \{I, X\}, \\ -1, & \alpha_e \in \{Y, Z\}, \end{cases} \quad (3.41)$$

and similarly for each face p :

$$B_p(\vec{\alpha}) = \prod_{e \in \partial(p)} F(\alpha_e), \quad F(\alpha_e) = \begin{cases} +1, & \alpha_e \in \{I, Z\}, \\ -1, & \alpha_e \in \{X, Y\}. \end{cases} \quad (3.42)$$

4. **Decoder:** We count the error weight $\text{wt}(\vec{\alpha})$ (number of non-identity entries). If $\text{wt}(\vec{\alpha}) \leq 1$, we declare the error *correctable*. Otherwise, we declare a decoding failure (for our simple demonstration).
5. **Performance metrics:** Compare the fidelity F_{enc} of the code to that of a single unencoded qubit F_{unenc} under the same noise. We can gather syndrome histograms to see how often each star/plaquette pattern arises.

Error Detection When an error occurs on a physical qubit (for example, a Pauli Z error), it will anticommute with some of the stabilizer operators. This leads to a change in the measurement outcome (from $+1$ to -1) for the stabilizers that overlap with the error. Concretely:

- A Z error on an edge will anticommute with the star operators (since $\{Z, X\} = 0$) on the vertices connected by that edge. Thus, the eigenvalue of A_v for those vertices will flip to -1 .
- Similarly, an X error will anticommute with the plaquette operators (since $\{X, Z\} = 0$), flipping the eigenvalues of B_p on the adjacent faces.

The pattern of these -1 outcomes is called the *syndrome*. The syndrome does not reveal the exact location of the error uniquely but gives enough information to deduce a likely error chain. Now we construct the error probability. Let p be the probability of a nontrivial (X, Y , or Z) error on a given qubit after each two-qubit gate. We assume the typical depolarizing channel:

$$\mathcal{E}(\rho) = (1-p)\rho + \frac{p}{3}(X\rho X + Y\rho Y + Z\rho Z). \quad (3.43)$$

Kitaev's code automatically protects against a large class of such errors, provided these errors are sufficiently sparse. The *syndrome* is given by measuring the eigenvalues A_v and B_p (each ± 1). One can attempt decoding by pairing up vertex defects and face defects in an optimal way.

Let the ideal (error-free) state be $\rho_0 = |\psi\rangle\langle\psi|$. Since the Pauli operators map $|\psi\rangle$ to states orthogonal to $|\psi\rangle$ (or at least to states that are not proportional to $|\psi\rangle\langle\psi|$), the only contribution to the fidelity comes from the identity operation. Thus, the fidelity is given exactly by

$$F_{\text{unenc}} = \text{Tr}\left(\rho_0 \mathcal{E}(\rho_0)\right) = (1 - p) \cdot \text{Tr}(\rho_0^2) + \frac{p}{3} \sum_{P \in \{X,Y,Z\}} \text{Tr}\left(\rho_0 (P \rho_0 P)\right). \quad (3.44)$$

Since ρ_0 is pure we have $\text{Tr}(\rho_0^2) = 1$, and for each non-identity Pauli error, $\text{Tr}(\rho_0 (P \rho_0 P)) = 0$. Therefore, the unencoded fidelity is exactly

$$F_{\text{unenc}} = 1 - p. \quad (3.45)$$

In the toric code, the logical qubit is encoded into $n = 2L^2$ physical qubits. For our simulation with $L = 2$, we have $n = 8$. Our simple decoding strategy declares an error correctable if the total error weight (i.e., the number of qubits that have experienced a non-identity error) is at most 1. The probability of having no errors is

$$P(0 \text{ errors}) = (1 - p)^8. \quad (3.46)$$

The probability of having exactly one error is

$$P(1 \text{ error}) = 8p(1 - p)^7. \quad (3.47)$$

Thus, the exact encoded fidelity, which we denote by F_{enc} , is given by

$$F_{\text{enc}} = (1 - p)^8 + 8p(1 - p)^7. \quad (3.48)$$

This expression is obtained directly by summing the probabilities of the error patterns that are deemed correctable by our decoder. We show the effects on fidelity and syndrome measurement with the following figures:

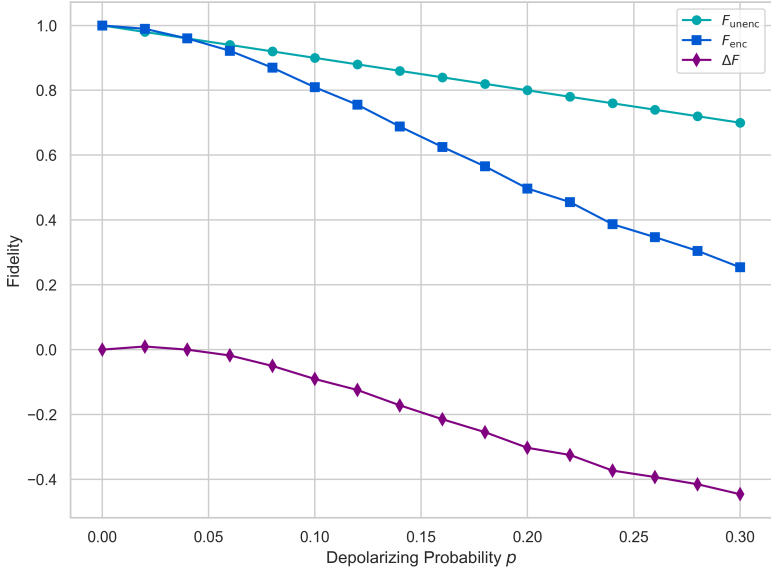


Figure 3. Error Correction Performance for Topological Codes The plot compares the fidelity of a logical qubit encoded in the toric code (F_{enc}) with that of a bare (unencoded) qubit (F_{unenc}) as a function of the physical error probability p . The significant improvement in F_{enc} demonstrates how the nonlocal stabilizer measurements of the toric code protect the encoded information against local errors.

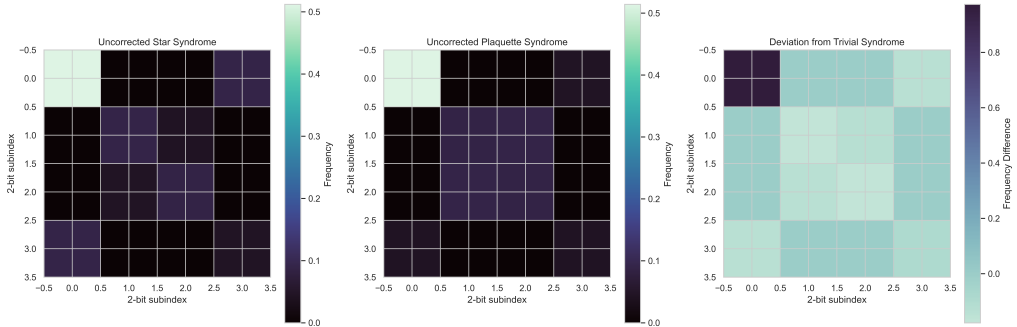


Figure 4. Syndrome Distribution in Toric Codes. The composite figure displays (a) the measured star (vertex) syndrome outcomes, (b) the plaquette syndrome outcomes, and (c) the difference from the ideal (trivial) syndrome pattern. These syndrome measurements reveal the locations of local errors, which are then corrected by the code’s decoder. In this way, the toric code effectively restores the logical state by detecting and mitigating errors through its topological stabilizers.

3.1.3 Replica Topological Quantum Error Correction

In practical fault-tolerant schemes one typically encodes logical qubits using topological codes (e.g. surface codes) rather than simple repetition codes. In this section, we extend our replica error mitigation framework to a topological quantum error correction model based on the rigorous framework of Kitaev’s toric code. For concreteness, we consider a

toric code defined on a 2×2 lattice on the torus, so that the number of physical qubits is $n = 8$. The code space is given by:

$$\mathcal{L} = \left\{ |\Psi\rangle \in (\mathbb{C}^2)^{\otimes 8} : A_s |\Psi\rangle = |\Psi\rangle, \quad B_p |\Psi\rangle = |\Psi\rangle, \quad \forall s, p \right\}, \quad (3.49)$$

with the stabilizer operators:

$$A_s = \prod_{j \in \text{star}(s)} \sigma_j^x, \quad B_p = \prod_{j \in \text{boundary}(p)} \sigma_j^z. \quad (3.50)$$

A simple decoder that corrects the code when at most one physical qubit error occurs yields an exact encoded fidelity:

$$F_{\text{enc}} = (1-p)^8 + 8p(1-p)^7, \quad (3.51)$$

where p is the error probability of the single-qubit depolarizing channel acting after each gate (with unencoded fidelity $F_{\text{unenc}} = 1-p$).

To further suppress residual errors, we now apply our replica virtual distillation procedure to the encoded state. That is, given the noisy encoded state ρ_{enc} , we construct the replicated state

$$\hat{\rho}_M = \frac{\rho_{\text{enc}}^M}{\text{Tr}(\rho_{\text{enc}}^M)}. \quad (3.52)$$

Analogously to our earlier treatment of the qutrit model, the effective fidelity with respect to the ideal encoded state is given by:

$$F_{\text{eff}}(M) = \frac{F_{\text{enc}}^M}{F_{\text{enc}}^M + 2^{1-M}(1-F_{\text{enc}})^M}. \quad (3.53)$$

Here the factor 2^{1-M} arises from the two-level nature of the physical qubits.

To quantify the benefit of this replica topological error correction scheme, we define two figures of merit:

- The *absolute fidelity improvement*:

$$\Delta F(M) = F_{\text{eff}}(M) - F_{\text{enc}}, \quad (3.54)$$

- The *relative fidelity improvement*:

$$R(M) = \frac{F_{\text{eff}}(M) - F_{\text{enc}}}{1 - F_{\text{enc}}}. \quad (3.55)$$

Here $\Delta F(M)$ captures the direct increase in fidelity resulting from the replication protocol compared to the original encoded state, thereby quantifying the net gain in preserving the ideal state. As for $R(M)$, by normalizing the fidelity gain with respect to the gap between the encoded fidelity and perfection, this measure expresses the improvement as a fraction of the maximum possible correction, allowing for meaningful comparisons across different error regimes.

In our numerical simulations we vary the physical error probability $p \in [0, 1]$ and the replica count $M \in \{1, \dots, 10\}$, compute F_{enc} from the surface code decoder via

$$F_{\text{enc}} = (1 - p)^8 + 8p(1 - p)^7, \quad (3.56)$$

and then evaluate $F_{\text{eff}}(M)$. Figures 5 and 6 (presented below) show 3D surface plots of the absolute and relative fidelity improvements as functions of p and M .

These results demonstrate that, even for a topologically encoded logical qubit, the replica virtual distillation protocol leads to a significant suppression of errors. In particular, for a given noise level, the effective fidelity improves exponentially with the number of replicas, thereby combining the strengths of topological error correction and quantum error mitigation.

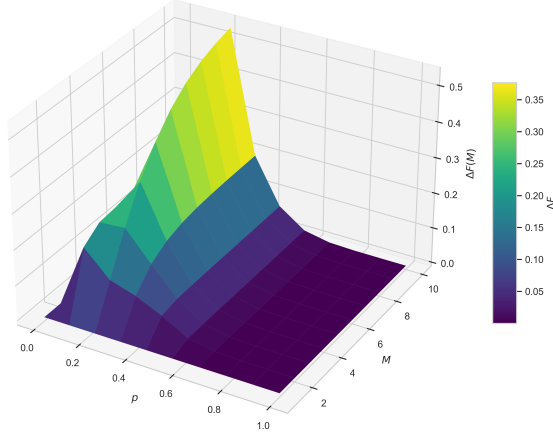


Figure 5. Absolute Fidelity Improvement $\Delta F(M)$: This 3D surface plot displays the absolute improvement in fidelity, defined as $\Delta F(M) = F_{\text{eff}}(M) - F_{\text{enc}}$, over a range of noise probabilities p (from 0 to 1) and replica counts M (from 1 to 10). The plot demonstrates that for a given baseline error-corrected fidelity F_{enc} , the replication protocol via virtual distillation yields a significant absolute increase in fidelity as M increases. Each data point is based on 10,000 simulation runs.

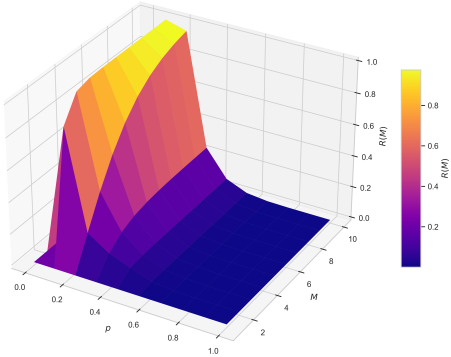


Figure 6. Relative Fidelity Improvement $R(M)$: This 3D surface plot illustrates the relative fidelity improvement, defined as $R(M) = \frac{F_{\text{eff}}(M) - F_{\text{enc}}}{1 - F_{\text{enc}}}$, as a function of noise probability p (ranging from 0 to 1) and replica count M (from 1 to 10). The relative improvement quantifies the enhancement provided by the replication protocol in comparison to the maximum possible improvement (i.e., the gap between F_{enc} and 1). Each value is computed from 10,000 simulation runs.

Now, we have defined the improvement for error correction with replicas as: $\Delta F = F_{\text{eff}}(M) - F_{\text{enc}}$. Renaming that to ΔF_{enc} , we may also define the quantities:

- $\Delta F_{\text{rep}} = F_{\text{eff}}(M) - F_{\text{rep}}(M)$, where $F_{\text{eff}}^{\text{rep}}(M)$ is the effective fidelity computed from the unencoded (replica-only) state.
- The residual error, $E(M) = 1 - F_{\text{eff}}(M)$, after applying virtual distillation.

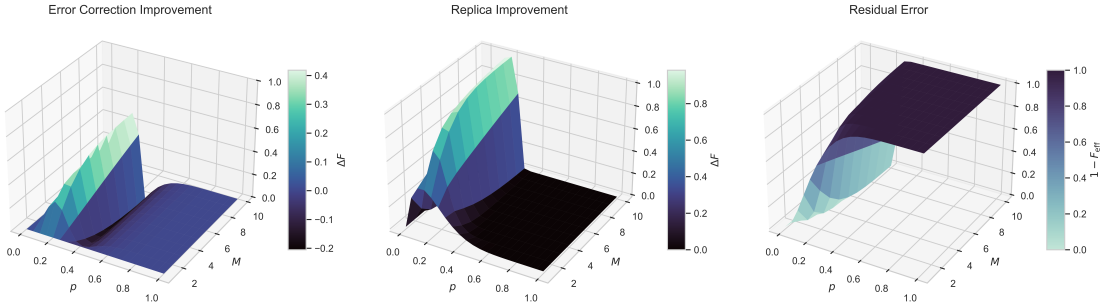


Figure 7. (a) Absolute fidelity improvement, $\Delta F = F_{\text{eff}}(M) - F_{\text{enc}}$, where F_{enc} is the fidelity of the encoded (error-corrected) state and $F_{\text{eff}}(M)$ is the effective fidelity after applying virtual distillation using M replicas. (b) Combined versus replica-only improvement, $\Delta F_{\text{comb}} = F_{\text{eff}}(M) - F_{\text{eff}}^{\text{rep}}(M)$, where $F_{\text{eff}}^{\text{rep}}(M)$ is the effective fidelity obtained from the unencoded (replica) state. (c) Residual error after the combined method, given by $1 - F_{\text{eff}}(M)$. In all panels, the horizontal axis corresponds to the single-qubit error rate $p \in [0, 1]$, the vertical axis to the replica count $M \in [0, 10]$, and the color scales (sequential for (a) and (b), diverging for (c)) span the relevant numerical range.

3.1.4 Relative Scaling Gain

In the previous subsections we demonstrated how replication with virtual distillation can improve the fidelity of an encoded logical state for a simple *qutrit* repetition code. In realistic fault-tolerant quantum computation, one typically uses topological codes such as Kitaev's toric code. In this section we rework the analysis of the relative scaling gain for quantum error correction within the rigorous framework of the toric code.

For concreteness we consider the toric code defined on a 2×2 square lattice on the torus. In this case the physical qubits reside on the 8 edges, and a simple decoding strategy based on single-qubit errors gives the exact encoded fidelity

$$F_{\text{enc}} = (1 - p)^8 + 8p(1 - p)^7, \quad (3.57)$$

where p is the probability that a single physical qubit suffers a nontrivial error (following an error channel such as the depolarizing channel). We then define the logical error as

$$\varepsilon = 1 - F_{\text{enc}}. \quad (3.58)$$

When M independent copies of the encoded state are prepared and subsequently combined via virtual distillation, the effective (error-mitigated) fidelity is given by

$$F_{\text{eff}}(M) = \frac{F_{\text{enc}}^M}{F_{\text{enc}}^M + 2^{1-M}(1 - F_{\text{enc}})^M}. \quad (3.59)$$

Thus, the residual error after applying virtual distillation becomes

$$\varepsilon_{\text{eff}} = (M)\varepsilon = (M)(1 - F_{\text{eff}}(M)). \quad (3.60)$$

To quantify the gain obtained by using replication rather than simply scaling up the individual code block, we define the scaling gain metric as the ratio

$$G(M) = \frac{1 - F_{\text{enc}}}{1 - F_{\text{eff}}(M)} = \frac{\varepsilon}{\varepsilon_{\text{eff}}(M)}. \quad (3.61)$$

Using the expression for $F_{\text{eff}}(M)$, one may show that

$$G(M, \varepsilon) = \frac{\varepsilon(F_{\text{enc}}^M + 2^{1-M}\varepsilon^M)}{2^{1-M}\varepsilon^M}. \quad (3.62)$$

This is defined as the ratio of the initial error to the residual error after replication, offering a rigorous quantitative measure of how effectively the replication strategy suppresses errors. In the limit where $\varepsilon \ll 1$ (i.e., the encoded state is of high fidelity) and for moderate values of M , we have the simplified scaling

$$G(M) \sim 2^{M-1} \varepsilon^{1-M}. \quad (3.63)$$

This relation indicates that, for a fixed baseline logical error ε , the advantage provided by virtual distillation increases exponentially with the number of copies M . In other words, even if a large improvement may be achieved by increasing the code distance (which

typically yields only polynomial improvements), the replication method can in principle yield a dramatic, super-exponential suppression of errors. This is shown in the following figure:

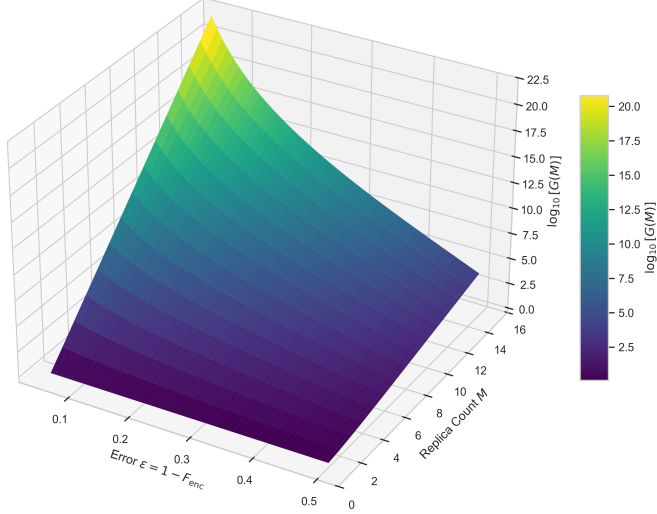


Figure 8. Logarithm of the Full Scaling Gain $G(M, \varepsilon)$: This 3D surface plot shows $\log_{10}[G(M, \varepsilon)]$ as a function of the error rate ε and the replica count M . Notably, the plot reveals that substantial scaling gains occur for small values of ε , confirming the superiority of the replication strategy over traditional code scaling.

3.2 Holographic Replica QEC

Placeholder for extending this framework to holographic theories such as AdS/CFT.

A Appendix

A.1 Qutrit Quantum Error Correction

A.2 Preliminary Frameworks